

Research Article

Parametric Analysis and Optimization of TIG Welding for Enhanced Structural Integrity of Mild-Steel Sktm13a Pipe Butt Joints

Sunny Itaofu Iremia* , Izelu Christoper Okechukwu ,
Omonigho Benedict Otanocha 

Mechanical Engineering, Federal University of Petroleum Resources, Warri, Nigeria

Abstract

The structural integrity of welded joints are critical factors that influence the overall safety and durability of various engineering structures, especially in the fields of construction, automotive, and pipeline industries.. This research systematically investigate the effects and interactions of welding parameters such as welding current, welding voltage, gas flow rate and welding speed for enhanced structural integrity of mild-steel SKTM13A pipe butt joints. Central Composite Design (CCD) based Response Surface Methodology (RSM) was used to investigate and optimized these Tungsten Inert Gas (TIG) welding process dependent variables to minimize responses such as residual stress, distortion in weld-ment, heat flux, and maximize Peak Temperature, tensile strength of the welded joints. The results indicated model F-values of 29.81 at a P-value of <0.0001 for the tensile strength explained the significance of the employed model. Optimal tensile strength of 308.56Mpa, minimum distortion in weldment of 0.2, Peak Temperature of 1518.45 °C, residual stress of 282.724Mpa and heat flux of 1500.26Kw/min were achieved at a welding current of 140A, welding voltage 24V, gas flow rate 12lit/min and welding speed of 150 cm/min. Overall, these statistics suggest that the regression model for the desired responses are robust and adequately captures the relationship with the predictor variables. In conclusion, this research has provided valuable insights into the optimization of welding parameters using Response Surface Methodology (RSM) that can be effectively apply to drive

Keywords

Analysis, Optimization, Parametric, Structural Integrity, TIG, Pipe

1. Introduction

The structural integrity and performance of welded joints are critical factors that influence the overall safety and durability of various engineering structures, especially in the fields of construction, automotive, and pipeline industries. Mild steel, known for its excellent weldability and mechanical properties, is commonly used in these applications. However,

achieving optimal weld quality through Tungsten Inert Gas (TIG) welding, particularly in multi-pass weldments of mild steel pipe butt joints, presents significant challenges. These challenges are rooted in managing the thermal effects induced by the welding process, which directly impact the residual stresses and distortion of the weldment [1]. Optimiza-

*Corresponding author: iremia2000@yahoo.co.uk (Sunny Itaofu Iremia)

Received: 14 January 2025; Accepted: 27 January 2025; Published: 21 February 2025



Copyright: © The Author(s), 2025. Published by Science Publishing Group. This is an **Open Access** article, distributed under the terms of the Creative Commons Attribution 4.0 License (<http://creativecommons.org/licenses/by/4.0/>), which permits unrestricted use, distribution and reproduction in any medium, provided the original work is properly cited.

tion of welding parameters is essential for enhancing the quality and structural integrity of weldments.

The welding of mild steel, particularly through the TIG (Tungsten Inert Gas) process, is a critical operation in the manufacturing, construction, and pipeline industries due to its impact on the structural integrity and performance of the welded components. While TIG welding is favored for its ability to produce high-quality, clean welds with minimal spatter [2], the process is not without its challenges. One of the primary concerns in TIG welding is the management of thermal input to prevent adverse effects such as excessive residual stresses and distortion, which can significantly compromise the mechanical properties and longevity of the weld [3]. This research systematically investigate the effects and interactions of welding parameters such as welding current, welding voltage, gas flow rate and welding speed for enhanced structural integrity of mild-steel SKTM13A pipe butt joints using the Central Composite Design (CCD) based Response Surface Methodology (RSM).

2. Literature Review

Despite the vast array of studies on welding processes, there remains a significant gap in research specifically addressing the optimization of TIG welding parameters for multi-pass weldments on mild steel pipe butt joints. These parameters, including welding current, voltage, and gas flow rate, are crucial for controlling the Heat Flux and, consequently mechanical properties of the weld [4]. Moreover, while computational models have been extensively applied to predict outcomes in welding [5], there is a notable shortage of studies that validate these models against experimental data, especially in the context of multi-pass TIG welding of mild steel.

Parametric optimization using advanced algorithms has shown promise in various welding applications [6], yet its application to TIG welding of mild steel requires further exploration. Tungsten Inert Gas (TIG) welding, also known as Gas Tungsten Arc Welding (GTAW), has been the subject of extensive research aimed at understanding and optimizing the process to improve weld quality and performance. The literature reveals a concerted effort to investigate various aspects of the TIG welding process, including the effects of Heat Flux, shielding gas, electrode type, and welding speed on the resultant weld properties.

Several researchers conducted detailed studies on the optimization of TIG welding parameters for stainless steel, highlighting the critical role of current and gas flow rate in determining the quality of the weld bead [7-13]. Their work

demonstrated that precise control over these parameters could significantly enhance the mechanical properties and surface finish of the weld. Achebo and [14-26] focused on the application of Design of Experiments (DoE) and Response Surface Methodology (RSM) in optimizing TIG welding parameters for mild steel. Their research demonstrated the effectiveness of these statistical tools in developing predictive models and optimizing welding conditions to achieve desired weld characteristics [27-36] examined the thermal and mechanical behavior of TIG weldments using advanced computational modeling techniques. Their study provided insights into the heat distribution and stress development during welding, contributing to a better understanding of the factors that influence weld integrity. Gas Tungsten Arc Welding (GTAW), commonly known as Tungsten Inert Gas (TIG) welding, has been extensively studied due to its versatility and ability to produce high-quality welds in various materials. [37] conducted research specifically focused on GTAW, exploring its application, process parameters, and effects on weld properties. Their study delved into the intricate relationship between welding parameters such as current, voltage, and shielding gas flow rate, and the resulting weld bead profiles and mechanical properties. By systematically varying these parameters and conducting experimental analyses, Palani and Saju were able to characterize the influence of each parameter on the geometry and quality of the weld bead. Tig welding is widely used in the fabrication industry but the process dynamics such as management of thermal input and optimal parameter settings are not fully understood due to its complexity. This research contributes to filling this knowledge gap. The study also demonstrates the efficacy of experimental design methodologies, such as DoE and RSM, in systematically exploring the effects of welding parameters and optimizing the welding process for improved performance and quality. By leveraging these techniques, researchers can gain valuable insights into the complex relationships between process variables and weld properties, leading to more efficient and reliable welding processes with enhanced mechanical and metallurgical properties.

3. Materials and Methodology

The study involving the Parametric Analysis and Optimization of TIG Weldment of Mild Steel pipe butt Joint for Improved Structural Integrity, was carried out using Response Surface Methodology (RSM). The material used for Tugsten Inert Gas welding is mild steel STKM13A pipe and the G2Si1 filler electrod with the following details as shown in Table 1.

Table 1. Composition (wt. %) of Mild steel STKM13A pipe and G2Si1 filler electrode.

Alloys	%	C	Cu	Fe	Mn	N	P	S	
STKM13A	Max	0.15	0.4	98.293	1.1	.01	0.02	0.027	
Alloys	%	C	Fe	Mn	Al	Mo	Ni	Si	Ti
G2Si1 electrode	Max	0.1	97.68	1.1	0.02	0.15	0.15	0.65	0.15

The key input parameters considered in this work are welding current, welding voltage, gas flow rate and welding speed with experimental process parameter ranges given in Table 2.

Table 2. Range and Levels of independent variables.

Parameters	Unit	Symbol	Coded value Low (-1)	Coded value High (+1)
Current	Amp	A	140	160
Voltage	Volt	V	20	24
Welding speed	cm/min	S	150	170
Gas flow rate	Lit/min	F	12	14

3.1. Response Surface Methodology (RSM) Analysis

The response or measured parameters includes; Peak Temperature, Residual Stress, Distortion in Weldment, Heat Flux and Tensile Strength. The range and level of the experimental variables were obtained from literature and are presented in Table 2.

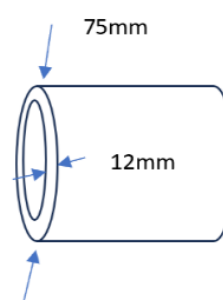
3.2. Design of Experiments (DoE)

The objective of the Design of Experiments (DoE) is to systematically investigate the effects of key TIG welding parameters on the structural integrity of mild steel pipe butt joints. This study aims to optimize these parameters to enhance the weld quality and performance.

The central composite design (CCD) method is used to generate the experimental runs. CCD is a robust design method in RSM that includes factorial points, axial points, and center points to provide sufficient information for a quadratic model. In this study, 30 experimental runs were generated.

3.3. Sample Preparation

For the RSM analysis, mild steel pipes with a diameter of 75 mm and a thickness of 12 mm were used. As shown in Figure 1, the pipes were cut to the required length and bevelled at the edges to prepare for butt joint welding.

**Figure 1.** Sketch of mild steel pipe used for Butt joint welding.

The pipe surfaces and bevel edges were thoroughly cleaned to remove contaminants, and the pipes were aligned and held in place using welding fixtures to ensure precise alignment and correct gap maintenance. The TIG welding equipment shown in Figure 5 was calibrated according to the experimental parameters, and welding was performed with consistent technique and specified shielding gas flow. The welding process uses a shielding gas to protect the weld specimen from atmospheric interaction. For this study, 100% pure Argon gas was used. The weld samples were made from 12mm thickness of mild steel pipe; the pipe was cut to size with the power hacksaw.

The edges grinded and surfaces polished with emery paper and the joints welded. The samples preparation and welding were done at the Metallurgical Training Institute (MTI) 4Q2X+HGW, Owerri Rd. Layout, Obosi, Anambra State.

Figures 1, 2 and 3 shows sample preparation, finished coupons and welded joint respectively.



Figure 2. Sample preparation.



Figure 3. Finished coupon.



Figure 4. Welded joint.



Figure 5. TIG/MMA-250S Welding Machine and other Equipment.

Peak Temperature as well as heat flux across the weldment was measured using infrared thermometer and infrared thermography device shown in Figures 6 and 7. Multiple temperature readings along the weld provided comprehensive thermal profiles essential for understanding heat distribution. After welding, the joints were allowed to cool at a controlled rate, labelled with unique identifiers, and inspected for defects. These prepared samples were then used for further testing to measure responses such as residual stress, distortion, and tensile strength at Ahmadu Bello University Engineering and metallurgical Laboratory, Zaria ensuring reliable data for the RSM analysis.

Stress values were recorded at critical points to capture variations induced by welding parameters using the X-ray diffraction machine shown in Figure 8. The distortion in welded joints was quantified using precision measurement tools such as coordinate measuring machines (CMM) in Figure 9.

Tensile test specimens were prepared according to standardized procedures and subjected to tensile testing using universal testing machines (UTM) presented in Figure 3.



Figure 6. Fluke62 Max infrared thermometer.



Figure 7. FLIR System-GF304 thermography.



Figure 8. AutoMATE II X-ray diffraction device.

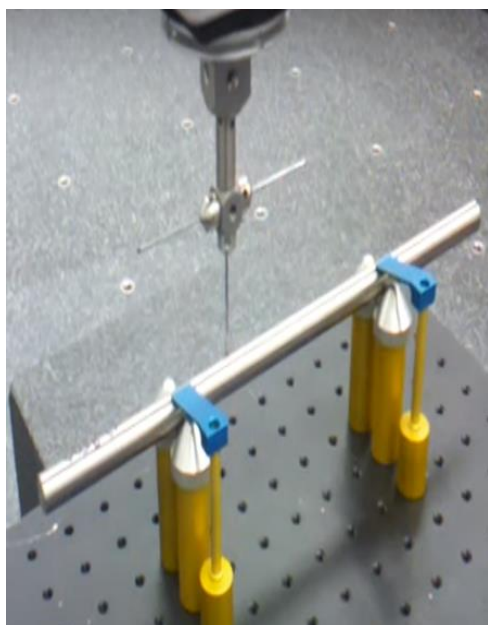


Figure 9. Coordinate Measuring machine (CMM).



Figure 10. M0565SHIMADZU UNIVERSAL TESTING MACHINE (UTM).

Repeat measurements and calibration checks were performed to validate the consistency of results. The collected data provided essential insights into the relationship between welding parameters and weld quality, enabling informed decision-making for process optimization and structural integrity enhancement. Table 3 shows the CCD experimental result obtained from the lab.

4. Experimental Results and Discussions

Table 3. CCD Experimental results.

Std	Run	Factor 1 A: Current A	Factor 2 B: Voltage V	Factor 3 C: Weld Speed cm/min	Factor 4 D: Gas Flow Rate Lit/min	Response 1 Temperature Distribution °C	Response 2 Residual Stress MPa	Response 3 Distortion in Weldment mm	Response 4 Heat Flux KW/m ²	Response 5 Tensile Strength MPa
15	1	140	24	170	14	1520.04	284.147	0.21	674.06	287.19
2	2	160	20	150	12	1519.66	266.105	0.22	873.61	271.96
16	3	160	24	170	14	1519.86	258.797	0.22	769.4	274.37
26	4	150	22	160	13	1519.88	259.18	0.22	760.34	281.32
5	5	140	24	150	12	1518.45	282.724	0.2	1500.26	308.56
21	6	150	18	160	13	1519.8	243.024	0.25	800.8	293.371

		Factor 1	Factor 2	Factor 3	Factor 4	Response 1	Response 2	Response 3	Response 4	Response 5
Std	Run	A: Current	B: Voltage	C: Weld Speed	D: Gas Flow Rate	Temperature Distribution	Residual Stress	Distortion in Weldment	Heat Flux	Tensile Strength
		A	V	cm/min	Lit/min	°C	MPa	mm	KW/m ²	MPa
23	7	150	22	140	13	1519.87	259.431	0.22	760.94	266.998
8	8	160	24	150	14	1519.86	259.79	0.22	769.4	277.705
22	9	150	26	160	13	1520.19	279.801	0.25	596.76	307.593
11	10	140	20	170	14	1519.64	255.67	0.22	882.22	286.857
13	11	140	24	170	12	1518.3	292.48	0.19	1577.54	304.463
20	12	150	22	160	15	1517.14	258.65	0.19	2179.4	294.781
10	13	160	20	170	12	1519.66	257.1	0.22	873.61	281.838
18	14	170	22	160	13	1519.7	253.52	0.22	853.87	269.128
17	15	130	22	160	13	1520.06	286.11	0.2	664.59	290.016
28	16	150	22	160	13	1519.23	259.18	0.22	1093.67	281.32
27	17	150	22	160	13	1519.23	259.18	0.22	1093.67	281.32
24	18	150	22	180	13	1519.8	259.18	0.22	800.53	281.32
19	19	150	22	160	11	1518.27	287.97	0.17	1593.36	305.61
4	20	160	20	150	14	1517.53	249.37	0.23	1976.99	268.224
9	21	140	20	170	12	1519.85	270.1	0.21	774.25	289.625
1	22	140	20	150	12	1519.85	270.1	0.21	774.25	284.86
12	23	160	20	170	14	1518.4	234.66	0.21	1524.4	293.84
30	24	150	22	160	13	1519.88	259.18	0.22	760.34	281.32
29	25	150	22	160	13	1519.88	259.18	0.22	760.34	281.32
7	26	140	24	150	14	1520.04	272.41	0.21	674.06	287.19
6	27	160	24	150	12	1520.07	272.55	0.21	659.65	287.91
25	28	150	22	160	13	1519.88	259.18	0.22	760.34	281.32
14	29	160	24	170	12	1520.07	272.55	0.21	659.65	287.91
3	30	140	20	150	14	1519.64	255.67	0.22	882.22	270.13

The Response Surface Methodology (RSM) study was built using version 13.0.5.0 and employed a randomized central composite design to develop a quadratic model. The study consisted of 30 runs without any blocks, indicating a

single experimental setup. This setup facilitated robust predictions and optimizations of welding process responses, contributing to the overall analysis presented in Table 4.

Table 4. Model Summary Statistics for individual responses.

Responses	Source	Std. Dev.	R ²	Adjusted R ²	Predicted R ²	PRESS
Peak Temperature	Linear	0.8340	0.0519	-0.0998	-0.4598	26.77
	2FI	0.6767	0.5256	0.2759	0.2108	14.47

Responses	Source	Std. Dev.	R ²	Adjusted R ²	Predicted R ²	PRESS	
Residual Stress	Quadratic	0.2723	0.9394	0.8828	0.7805	4.02	Suggested
	Cubic	0.3045	0.9646	0.8534	0.1838	14.97	Aliased
	Linear	5.83	0.8378	0.8119	0.7630	1240.67	
	2FI	5.15	0.9039	0.8533	0.8361	857.86	
	Quadratic	1.09	0.9966	0.9934	0.9803	103.24	Suggested
Distortion in weldment	Cubic	0.2655	0.9999	0.9996	0.9864	71.05	Aliased
	Linear	0.0151	0.1799	0.0486	-0.2708	0.0088	
	2FI	0.0170	0.2068	-0.2106	-0.3883	0.0096	
	Quadratic	0.0047	0.9532	0.9096	0.7306	0.0019	Suggested
	Cubic	0.0019	0.9964	0.9851	0.4820	0.0036	Aliased
Heat flux	Linear	432.55	0.0519	-0.0998	-0.4598	7.202E+06	
	2FI	350.97	0.5256	0.2759	0.2108	3.894E+06	
	Quadratic	141.21	0.9394	0.8828	0.7805	1.083E+06	Suggested
	Cubic	157.95	0.9646	0.8534	0.1838	4.027E+06	Aliased
	Linear	9.24	0.4247	0.3326	0.1138	3284.61	
Tensile Strength	2FI	8.61	0.6200	0.4200	0.3331	2471.51	
	Quadratic	3.24	0.9575	0.9179	0.7554	906.53	Suggested
	Cubic	3.18	0.9809	0.9208	-1.7539	10206.47	Aliased

Table 5. Fit Statistics for Individual Responses.

Responses	Std. Dev.	Mean	C.V. %	R ²	Adjusted R ²	Predicted R ²	Adeq Precision
Peak Temperature	0.2723	1519.46	0.0179	0.9394	0.8828	0.7805	14.6631
Residual Stress	1.09	264.57	0.4132	0.9966	0.9934	0.9803	75.7186
Distortion in Weldment	0.0047	0.2150	2.16	0.9532	0.9096	0.7306	25.8249
Heat Flux	141.21	977.48	14.45	0.9394	0.8828	0.7805	14.6630
Tensile Strength	3.24	285.31	1.14	0.9575	0.9179	0.7554	20.0008

Table 5 presents fit statistics for the response variables such as Peak Temperature, Residual stress, Distortion in weldment, Heat flux and Tensile strength. The "Std. Dev." column indicates the standard deviation of the residuals, which measures the dispersion of data points around the regression line. A lower standard deviation suggests less variability and better fit of the model to the data. The "R²" value represents the coefficient of determination, indicating the proportion of variance in the responses explained by the regression model. For example, Peak Temperature with an R² of 0.9394 suggests that approximately 93.94% of the variance in Peak Temperature is accounted for by the regression model. The "Adjusted R²" adjusts R² for the number of predictors in the model,

offering a more accurate assessment of model fit. In this case, the Adjusted R² of 0.8828 implies that the model retains its explanatory power even after considering the number of predictors. The "Predicted R²" provides an estimate of the model's predictive capability on new data, with a value of 0.7805 indicating a reasonably good prediction performance. Lastly, the "Adeq Precision" indicates the signal-to-noise ratio, suggesting that the model is adequate for making predictions, with a value of 14.6631. Overall, these statistics suggest that the regression model for Peak Temperature is robust and adequately captures the relationship with the predictor variables.

4.1. Individual Response ANOVA for Quadratic Modeling

Tables 6 to 10 present ANOVA for the different responses, each row corresponds to a different factor or interaction, including individual factors (A, B, C, D), their interactions (AB, AC, AD, BC, BD, CD), and the quadratic terms (A^2 , B^2 , C^2 , D^2), along with residual terms. The table shows the sum of squares, degrees of freedom, mean square, F-value, and p-value for each factor. The p-values indicate the significance

of each factor in explaining the variability in the response. Factors with p-values less than the significance level (usually 0.05) are considered significant. In this case, the quadratic terms and the interactions which have significant p-values, suggest that they significantly contribute to the variability in the response variables. Conversely, factors with non-significant p-values are considered not significant. The tables show that the model for each of the responses is significant with p-value less than 0.005 with lack of fit not significant.

Table 6. ANOVA for Peak Temperature.

Source	Sum of Squares	df	Mean Square	F-value	p-value	
Model	17.23	14	1.23	16.60	< 0.0001	significant
A-Current	0.0863	1	0.0863	1.16	0.2976	
B-Voltage	0.4401	1	0.4401	5.94	0.0278	
C-Weld Speed	0.0136	1	0.0136	0.1833	0.6747	
D-Gas Flow Rate	0.4125	1	0.4125	5.57	0.0323	
AB	2.85	1	2.85	38.48	< 0.0001	
AC	0.0652	1	0.0652	0.8801	0.3630	
AD	2.83	1	2.83	38.12	< 0.0001	
BC	0.0652	1	0.0652	0.8801	0.3630	
BD	2.81	1	2.81	37.97	< 0.0001	
CD	0.0652	1	0.0652	0.8801	0.3630	
A^2	0.1240	1	0.1240	1.67	0.2154	
B^2	0.2548	1	0.2548	3.44	0.0835	
C^2	0.0887	1	0.0887	1.20	0.2911	
D^2	6.22	1	6.22	83.86	< 0.0001	
Residual	1.11	15	0.0741			
Lack of Fit	0.5611	10	0.0561	0.5094	0.8297	not significant
Pure Error	0.5507	5	0.1101			
Cor Total	18.34	29				

Table 7. ANOVA for Residual Stress.

Source	Sum of Squares	df	Mean Square	F-value	p-value	
Model	5216.91	14	372.64	311.85	< 0.0001	significant
A-Current	1313.62	1	1313.62	1099.35	< 0.0001	
B-Voltage	1230.30	1	1230.30	1029.62	< 0.0001	
C-Weld Speed	1841.46	1	1841.46	1541.10	< 0.0001	
D-Gas Flow Rate	0.5757	1	0.5757	0.4818	0.4982	

Source	Sum of Squares	df	Mean Square	F-value	p-value	
AB	20.66	1	20.66	17.29	0.0008	
AC	35.31	1	35.31	29.55	< 0.0001	
AD	133.41	1	133.41	111.65	< 0.0001	
BC	32.71	1	32.71	27.37	0.0001	
BD	1.39	1	1.39	1.16	0.2977	
CD	122.19	1	122.19	102.26	< 0.0001	
A ²	192.15	1	192.15	160.81	< 0.0001	
B ²	339.96	1	339.96	284.50	< 0.0001	
C ²	8.18	1	8.18	6.85	0.0194	
D ²	0.0103	1	0.0103	0.0086	0.9272	
Residual	17.92	15	1.19			
Lack of Fit	17.92	10	1.79	0.5094	0.8297	not significant
Pure Error	0.0000	5	0.0000			
Cor Total	5234.83	29				

Table 8. ANOVA for Distortion in Weldment.

Source	Sum of Squares	df	Mean Square	F-value	p-value	
Model	0.0066	14	0.0005	21.84	< 0.0001	significant
A-Current	0.0005	1	0.0005	23.27	0.0002	
B-Voltage	0.0005	1	0.0005	23.27	0.0002	
C-Weld Speed	0.0002	1	0.0002	9.42	0.0078	
D-Gas Flow Rate	0.0000	1	0.0000	1.73	0.2081	
AB	0.0001	1	0.0001	2.60	0.1280	
AC	0.0001	1	0.0001	2.60	0.1280	
AD	6.250E-06	1	6.250E-06	0.2885	0.5991	
BC	0.0001	1	0.0001	2.60	0.1280	
BD	6.250E-06	1	6.250E-06	0.2885	0.5991	
CD	6.250E-06	1	6.250E-06	0.2885	0.5991	
A ²	0.0002	1	0.0002	10.01	0.0064	
B ²	0.0029	1	0.0029	134.63	< 0.0001	
C ²	0.0014	1	0.0014	65.40	< 0.0001	
D ²	2.679E-06	1	2.679E-06	0.1236	0.7300	
Residual	0.0003	15	0.0000			
Lack of Fit	0.0003	10	0.0000	0.5094	0.8297	not significant
Pure Error	0.0000	5	0.0000			
Cor Total	0.0069	29				

Table 9. ANOVA for Heat Flux.

Source	Sum of Squares	df	Mean Square	F-value	p-value	
Model	4.635E+06	14	3.310E+05	16.60	< 0.0001	significant
A-Current	23213.66	1	23213.66	1.16	0.2976	
B-Voltage	1.110E+05	1	1.110E+05	5.57	0.0323	
C-Weld Speed	1.184E+05	1	1.184E+05	5.94	0.0278	
D-Gas Flow Rate	3653.87	1	3653.87	0.1833	0.6747	
AB	7.601E+05	1	7.601E+05	38.12	< 0.0001	
AC	7.672E+05	1	7.672E+05	38.47	< 0.0001	
AD	17547.64	1	17547.64	0.8801	0.3630	
BC	7.570E+05	1	7.570E+05	37.97	< 0.0001	
BD	17547.64	1	17547.64	0.8801	0.3630	
CD	17547.64	1	17547.64	0.8801	0.3630	
A ²	33365.15	1	33365.15	1.67	0.2154	
B ²	1.672E+06	1	1.672E+06	83.86	< 0.0001	
C ²	68543.91	1	68543.91	3.44	0.0835	
D ²	23871.68	1	23871.68	1.20	0.2911	
Residual	2.991E+05	15	19939.18			
Lack of Fit	1.509E+05	10	15093.95	0.5094	0.8297	not significant
Pure Error	1.481E+05	5	29629.63			
Cor Total	4.934E+06	29				

Table 10. ANOVA for Tensile Strength.

Source	Sum of Squares	df	Mean Square	F-value	p-value	
Model	3548.83	14	253.49	24.16	< 0.0001	significant
A-Current	569.34	1	569.34	54.26	< 0.0001	
B-Voltage	362.53	1	362.53	34.55	< 0.0001	
C-Weld Speed	387.28	1	387.28	36.91	< 0.0001	
D-Gas Flow Rate	254.79	1	254.79	24.28	0.0002	
AB	103.34	1	103.34	9.85	0.0068	
AC	120.44	1	120.44	11.48	0.0041	
AD	13.62	1	13.62	1.30	0.2724	
BC	176.59	1	176.59	16.83	0.0009	
BD	50.63	1	50.63	4.83	0.0442	
CD	259.35	1	259.35	24.72	0.0002	
A ²	27.98	1	27.98	2.67	0.1233	
B ²	471.47	1	471.47	44.93	< 0.0001	
C ²	487.90	1	487.90	46.50	< 0.0001	

Source	Sum of Squares	df	Mean Square	F-value	p-value	
D ²	153.18	1	153.18	14.60	0.0017	
Residual	157.38	15	10.49			
Lack of Fit	157.38	10	15.74	0.5094	0.8297	not significant
Pure Error	0.0000	5	0.0000			
Cor Total	3706.22	29				

4.2. Model Equation Derived from RSM Analysis Using Design Expert 13

Table 11 present the model equations for the responses and describe how they are influenced by the linear terms current A, voltage B, weld speed C, and gas flow rate D, including their interactions and quadratic terms. The base Peak Temperature is 1546.34758 units. An increase in current slightly reduces the temperature, while an increase in voltage significantly raises it. Weld speed has a moderate negative effect, and gas flow rate has a negligible negative effect. Interaction terms like AB, AC, and BC show how combined changes in these factors impact the Peak Temperature, with AB and CD having a minor influence. The quadratic term B² has a substantial negative effect, indicating that higher voltage levels reduce Peak Temperature significantly. The other quadratic terms have minimal impact. The base level of residual stress is 1100.68047 units. The residual stress decreases with increasing current, voltage, and weld speed, as shown by the negative coefficients for these factors -0.948666, -92.65930, and -21.88771 respectively, while gas flow rate has a minor positive effect 1.59734. Interaction terms like AB -0.113633, AC -0.074277, and others indicate how combinations of these factors further influence residual stress, albeit slightly. Additionally, quadratic terms reveal nonlinear influences: for instance, B² 3.52054 significantly increases residual stress, whereas A² 0.026468 and C² 0.136542 have smaller positive effects. The model equation for distortion in weldment reveals a complex relationship between the variables and Distortion, with both positive and negative effects. The linear terms (0.010271A, 0.290208B, -0.111771C, 0.001937D) indicate the individual contributions of each variable, while the interaction terms (0.000187AB, 0.000094AC,

-6.25000E-06AD, 0.000938BC, -0.000062BD, 0.000031CD) show how the variables interact to influence Distortion. The quadratic terms (-0.000028A², -0.010312B², 0.001797C², -3.12500E-06D²) indicate non-linear relationships. Heat Flux has a base level of significantly negative value at -12969.61316 units, which adjusts with the contributions from the other factors. Current A and gas flow rate D have positive effects on Heat Flux with coefficients of 118.24231 and 149.46870 respectively, whereas voltage B and weld speed C show negative effects with coefficients of -6698.53799 and -3305.96649 respectively. The interaction terms such as AB (21.79631) and AC (-10.94841) show how combinations of these factors further influence the Heat Flux. Quadratic terms reveal non-linear effects, with B² (246.91003) significantly increasing the Heat Flux, while other quadratic terms like A² (-0.348775) and C² (-12.49749) have negative influences. The base tensile strength is 138.01713 units, adjusted by the contributions of the factors. Current A and gas flow rate D have positive effects on tensile strength, with coefficients of 0.780513 and 8.62017 respectively. In contrast, voltage B has a significant negative impact with a coefficient of -141.71908, while weld speed C positively affects tensile strength with a coefficient of 29.99611. Interaction terms such as AB (0.254139) and BC (-1.66111) indicate how combinations of these factors further influence tensile strength. Quadratic terms like B² (4.14596) and C² (1.05439) reveal the non-linear effects, suggesting that increases in voltage and weld speed lead to significant changes in tensile strength. Overall, this equation provides a detailed model of how various welding parameters and their interactions impact the tensile strength of the weldment.

In all, these equations allow for precise adjustments of welding parameters to control the different responses effectively.

Table 11. Final Equation in Terms of Actual Factors.

Actual Factors	Coefficients of actual factors in the responses				
	Peak Temperature=	Residual stress=	Distrtion in weldment =	Heat flux =	Tensile strength =
	+1546.34758	+1100.68047	-1.40031	-12969.61316	+138.01713
A-Current	-0.227975	-0.948666	+0.010271	+118.24231	+0.780513

Actual Factors	Coefficients of actual factors in the responses				
	Peak Temperature=	Residual stress=	Distrtion in weldment =	Heat flux =	Tensile strength =
B-Voltage	+12.91510	-92.65930	+0.290208	-6698.53799	-141.71908
C-Welding speed	-6.37405	-21.88771	-0.111771	+3305.96649	+29.99611
D-Gas flow rate	-0.28818	+1.59734	+0.001937	+149.46870	+8.62017
AB	-0.042024	-0.113633	-0.000187	+21.79631	+0.254139
AC	+0.021109	-0.074277	+0.000094	-10.94841	-0.137184
AD	+0.000639	-0.028876	-6.25000E-06	-0.331169	+0.009228
BC	+0.209692	+0.714883	+0.000938	-108.75906	-1.66111
BD	+0.209692	-0.029482	-0.000062	-3.31169	+0.177882
CD	-0.003193	+0.138173	+0.000031	+1.65584	-0.201306
A ²	+0.000672	+0.026468	-0.000028	-0.348775	-0.010099
B ²	-0.476054	+3.52054	-0.010312	+246.91003	+4.14596
C ²	+0.024096	+0.136542	-0.010312	-12.49749	+1.05439
D ²	+0.000569	+0.000194	-3.12500E-06	-0.295012	-0.023632

4.3. Predicted vs Actual Plots for the Responses

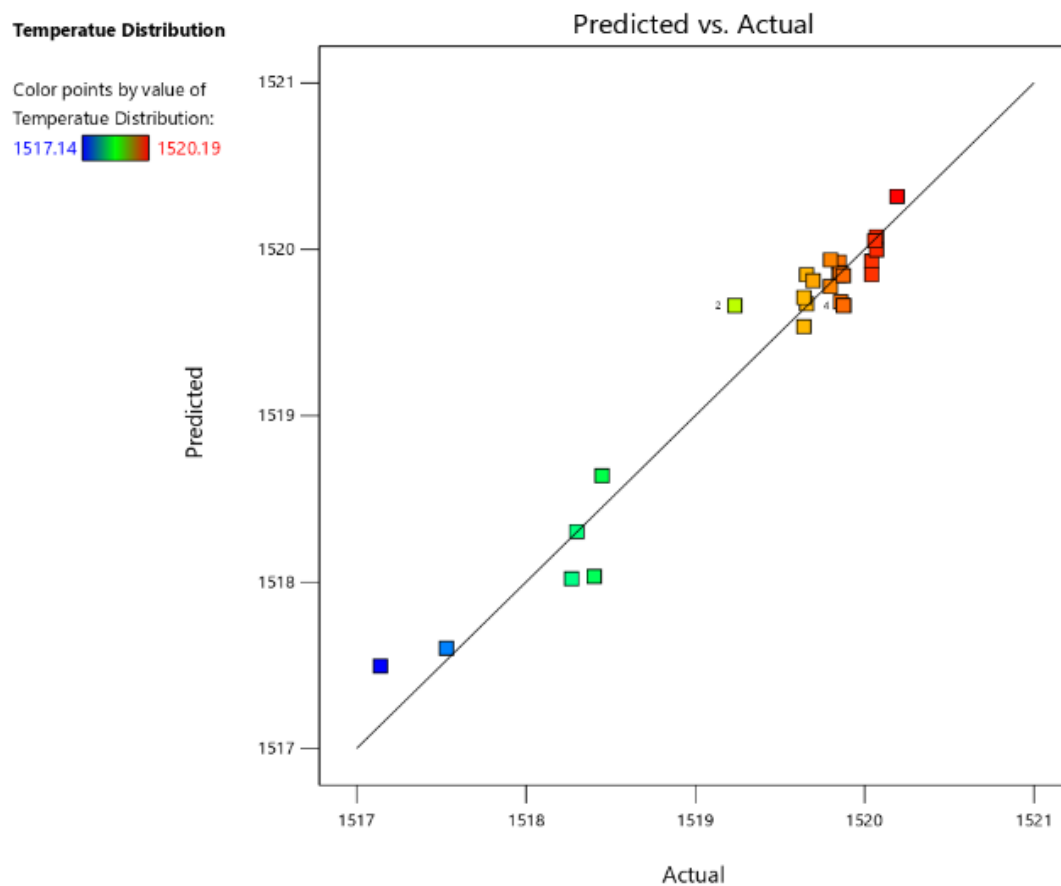


Figure 11. Peak Temperature.

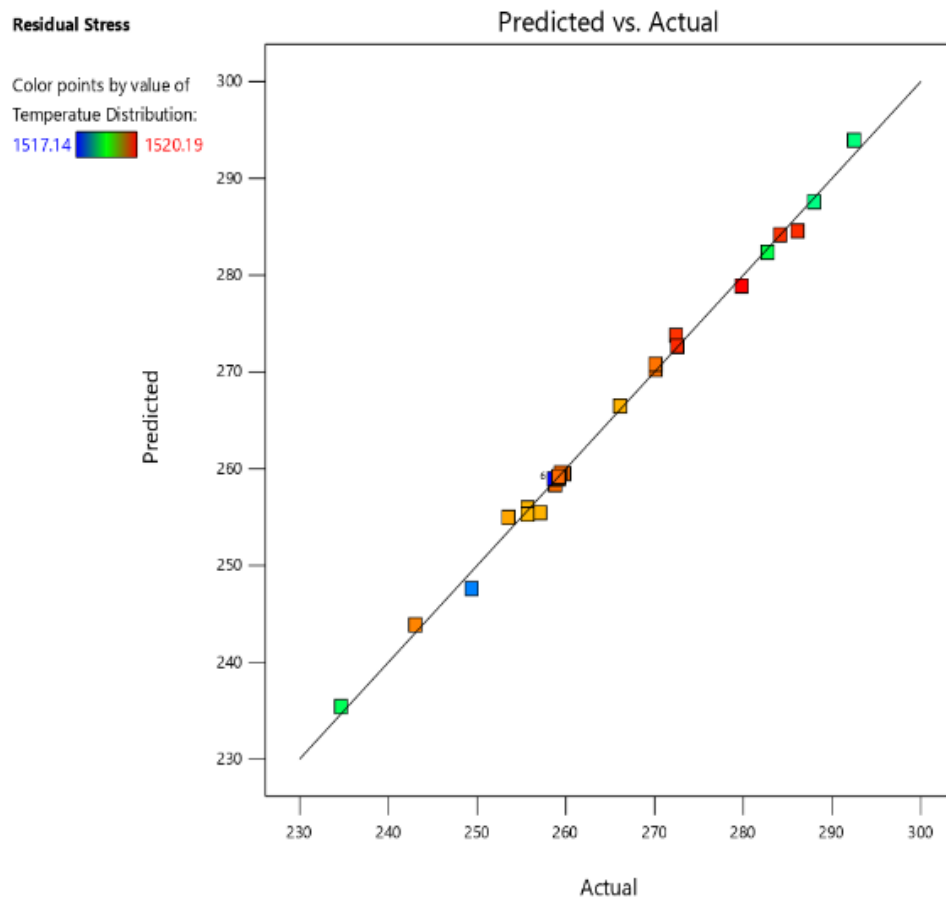


Figure 12. Residual stress.

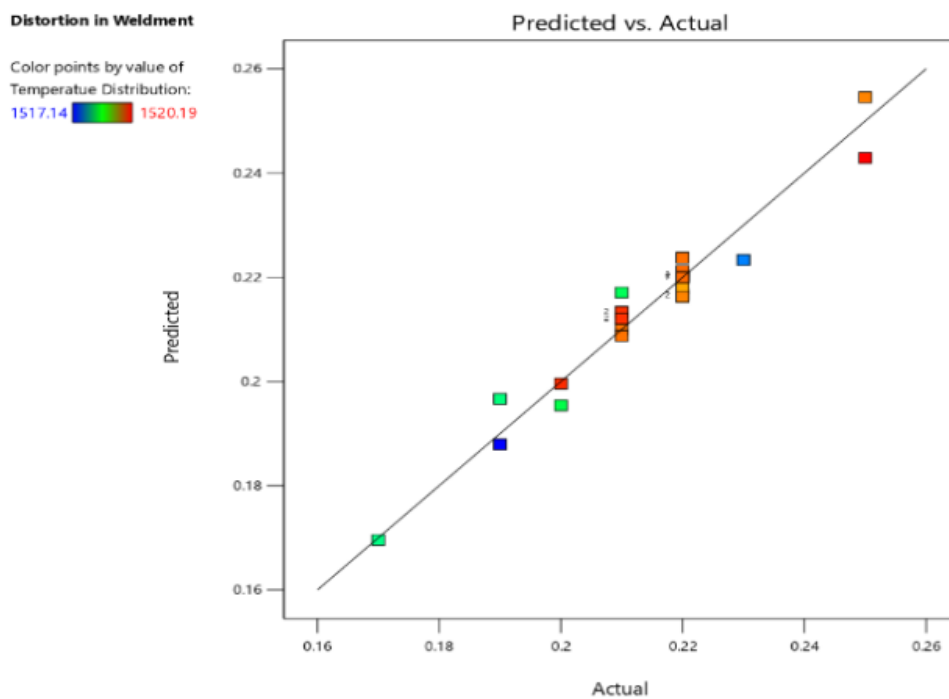


Figure 13. Distortion in weldment.

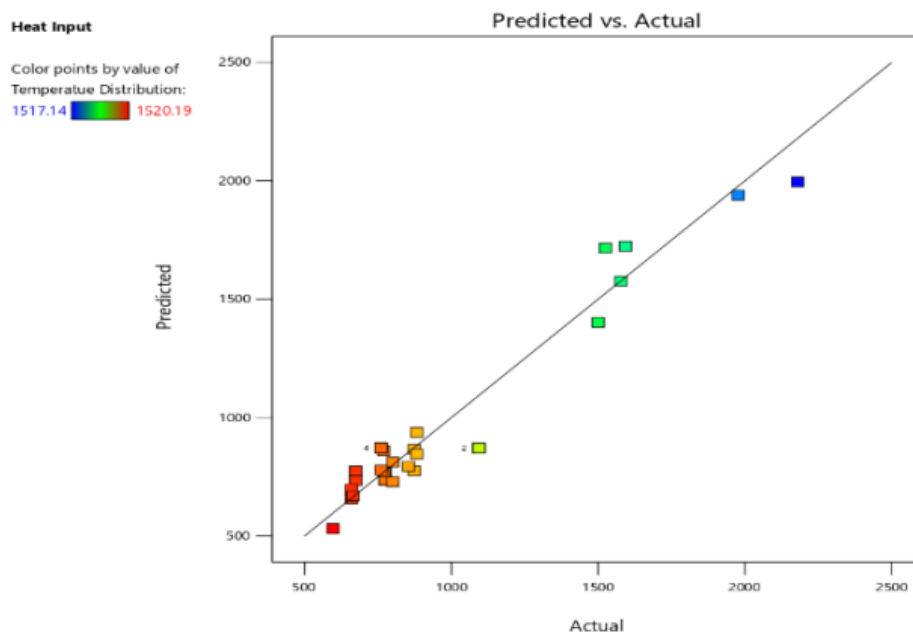


Figure 14. Heat flux.

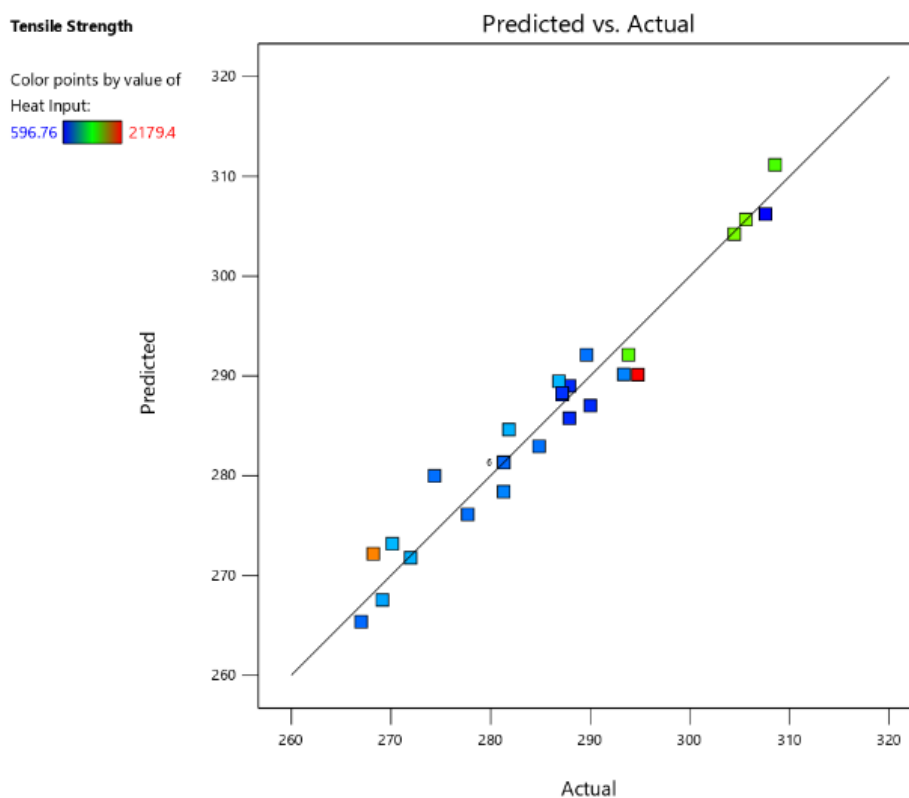


Figure 15. Tensile strength.

Figures 11-15, illustrate the relationship between the predicted values of the responses, Peak Temperature, residual stress, distortion in weldment, heat flux and tensile strength obtained from the regression model and the actual measured values. This plot is essential for evaluating the accuracy and reliability of the predictive model for each of the responses.

Ideally, the points should cluster closely around the diagonal line, indicating a strong agreement between the predicted and actual values. Deviations from this line suggest discrepancies between the predicted and observed values, which may indicate areas where the model requires refinement or where other unaccounted-for factors may be influencing the each of

the responses. Analyzing this plot helps assess the model's performance and identify areas for improvement in predicting each of the responses accurately.

4.4. Perturbation Plots for the Response Variables

The perturbation plot shows the comparative effects of the

independent variables at a particular point in the design space as shown in Figures 16 to 20. A significant steep slope or curvature of factors A, B, and D for instance in Figure 16, show that the Peak Temperature is mostly influenced by the gas flow rate, voltage and the current, The sensitivity of the independent variable to the response variables is explained by the steepness or higher slope of the factors in the perturbation plot.

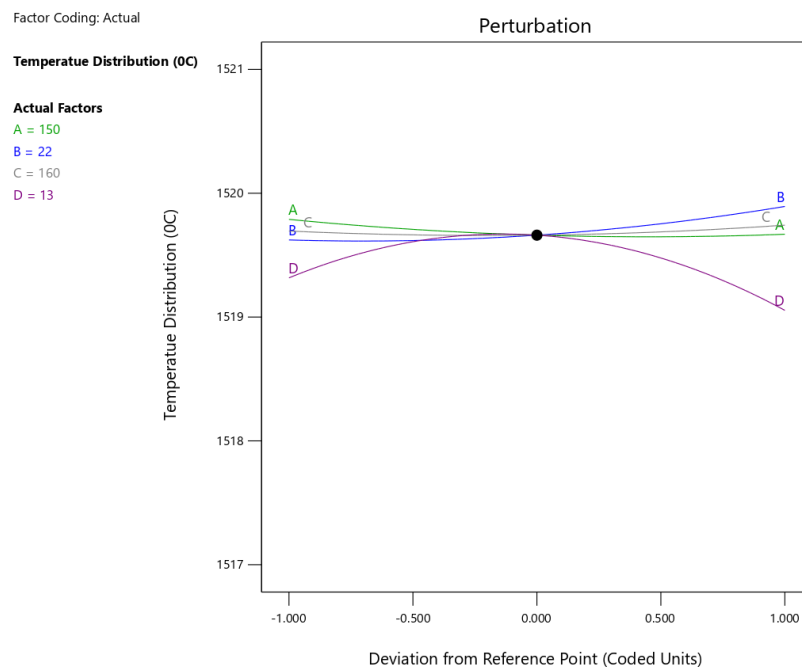


Figure 16. Perturbation plot for Peak Temperature.

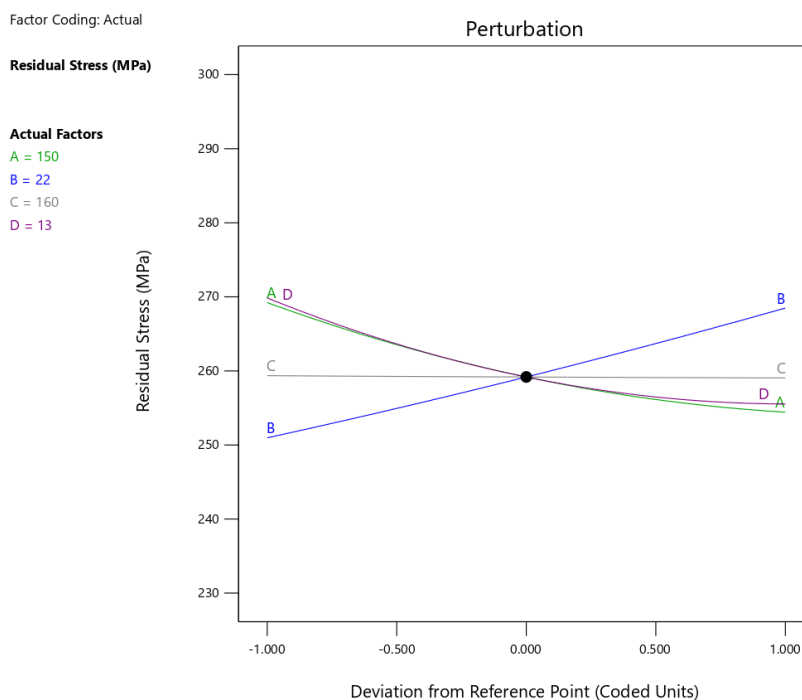


Figure 17. Perturbation plot for residual stress.

Factor Coding: Actual

Distortion in Weldment (mm)

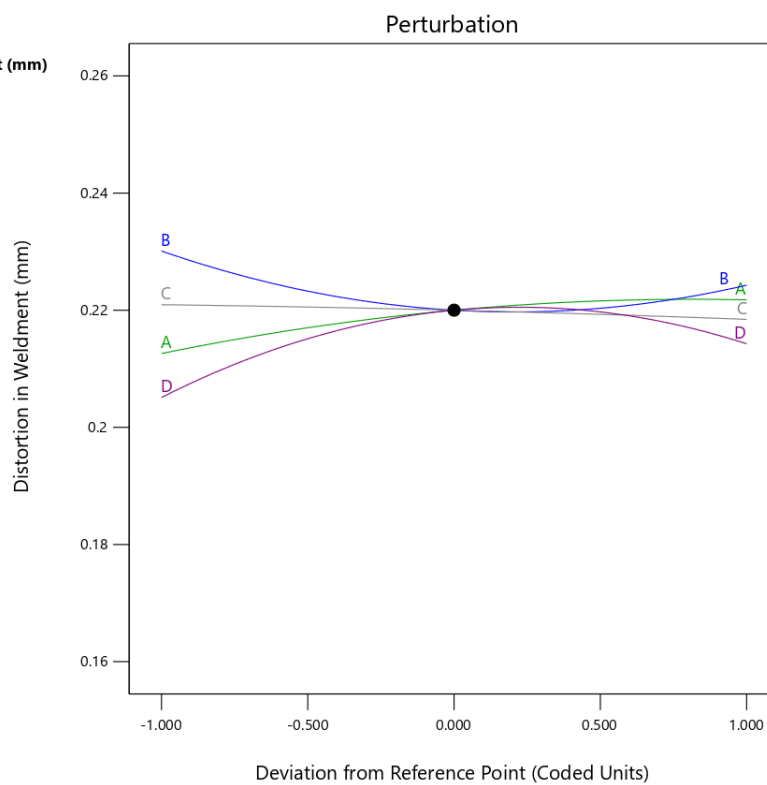
Actual Factors

A = 150

B = 22

C = 160

D = 13

*Figure 18. Perturbation plot for distortion in weldment.*

Factor Coding: Actual

Heat Flux (mm)

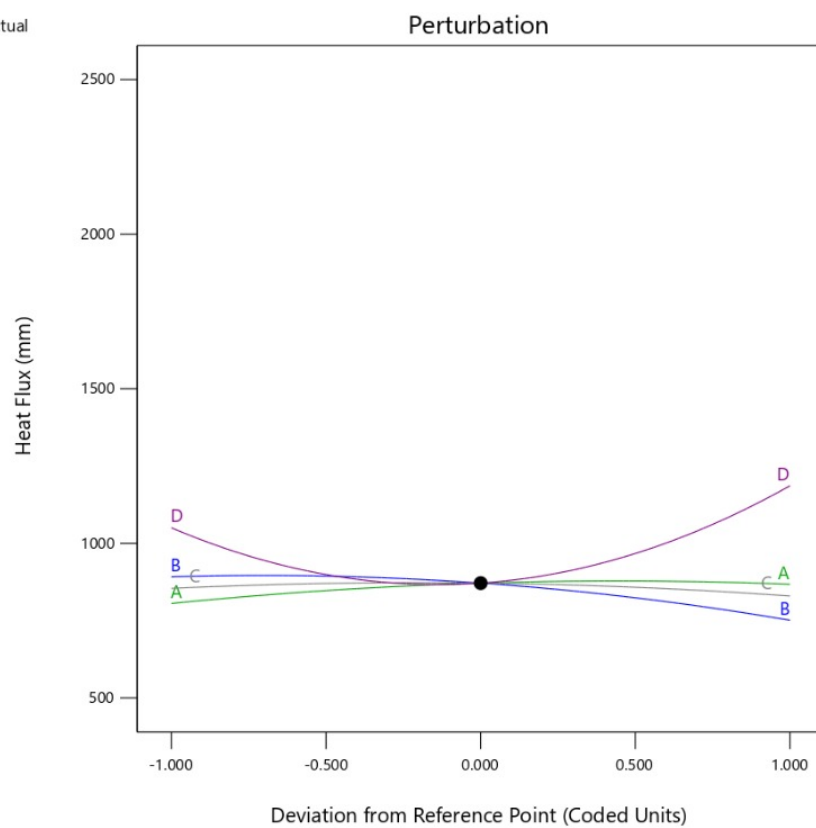
Actual Factors

A = 150

B = 22

C = 160

D = 13

*Figure 19. Perturbation plot for heat flux.*

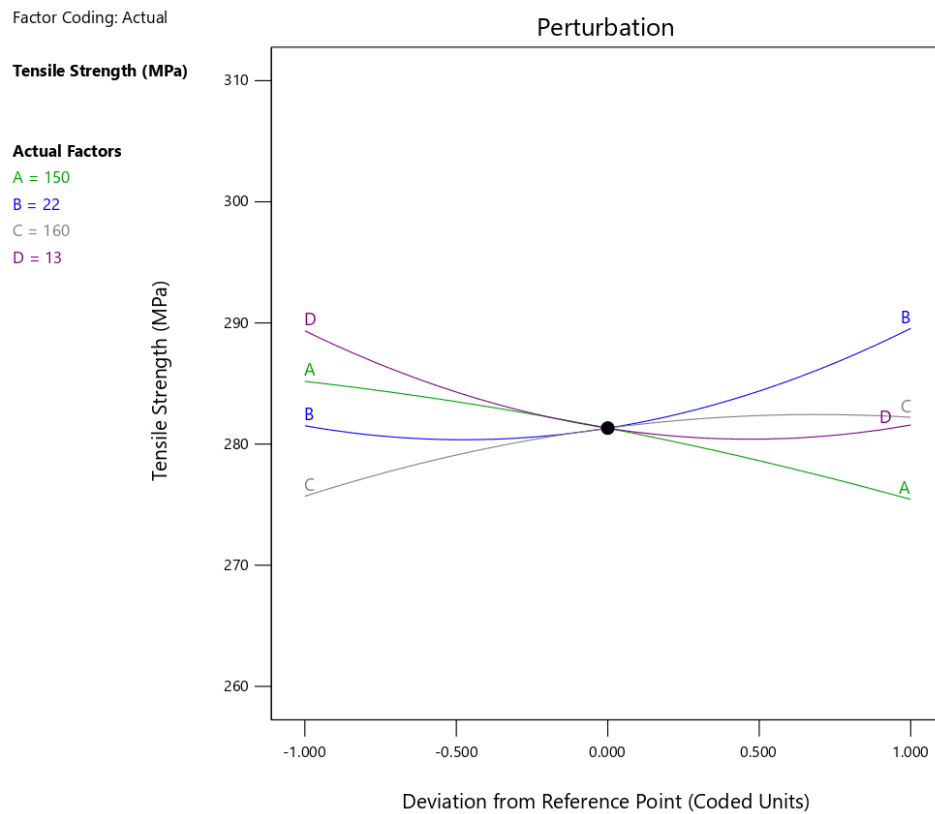


Figure 20. Perturbation plot for tensile strength.

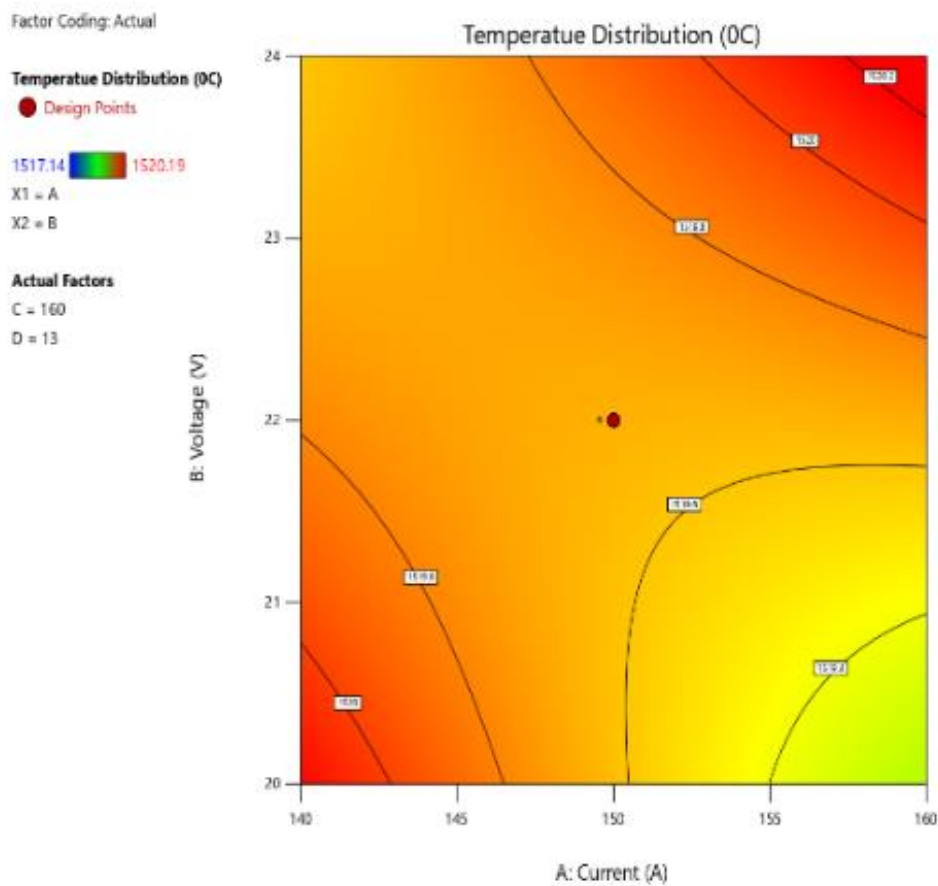


Figure 21. Contour plot for Peak Temperature.

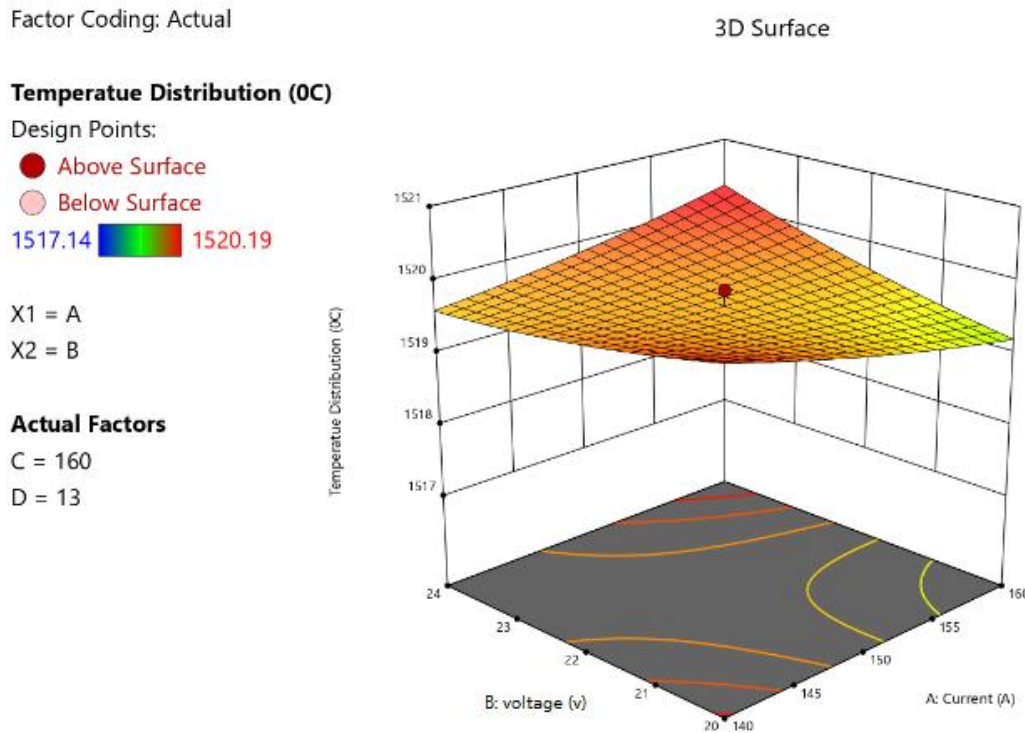


Figure 22. 3D surface plot for Peak Temperature.

Figure 21 depicts a contour plot illustrating the Peak Temperature across a welding process. Contour plots like this one are essential for understanding the spatial distribution of temperature within the welded component or structure. In this specific plot, different colors represent different temperature levels, with warmer colors indicating higher temperatures and cooler colors indicating lower temperatures. By analyzing this plot, engineers and researchers can identify regions of interest where temperature may be excessively high or low, allowing for adjustments to welding parameters or the design of cooling strategies to ensure uniform Peak Temperature and prevent issues like overheating or insufficient heat penetration, which could compromise the integrity of the weld. Figure 22 presents a 3D surface plot depicting the Peak Temperature within a welded structure. The plot provides a visual representation of how temperature varies across the surface, offering insights into the heat-affected zone and thermal gradients during the welding process. Understanding Peak Temperature is crucial for controlling metallurgical transformations and mechanical properties, as excessive heat can lead to undesirable outcomes such as distortion, residual stresses, and reduced mechanical strength. Engineers can use this plot to optimize welding parameters, ensuring uniform Peak Temperature for desired material properties and structural integrity in welded components.

Figure 23, presents a contour plot demonstrating the distribution of residual stress within a welded component or structure. Residual stress, which remains in a material after

the removal of external forces, can significantly affect the performance and longevity of welded structures. In this contour plot, different colors represent varying levels of residual stress, with warmer colors indicating higher stress levels and cooler colors indicating lower stress levels. Analyzing this plot enables engineers and researchers to identify regions of the weld where residual stress concentrations are particularly high, which may lead to issues such as cracking, distortion, or reduced fatigue life. By understanding and managing residual stress through appropriate welding techniques or post-weld heat treatments, engineers can enhance the structural integrity and performance of welded components. Figure 24 illustrates a 3D surface plot representing the distribution of residual stress within a welded structure. Residual stresses arise from thermal gradients and material shrinkage during the welding process, impacting the structural integrity and performance of welded components. This plot provides a visual depiction of how residual stresses vary across the surface, indicating regions of high and low stress concentrations. By analyzing this distribution, engineers can optimize welding procedures to minimize residual stresses, thereby reducing the risk of deformation, cracking, and premature failure in welded structures. Additionally, understanding the residual stress distribution enables the design of effective post-weld heat treatment or stress-relieving techniques to mitigate potential issues and enhance the overall performance of welded assemblies.

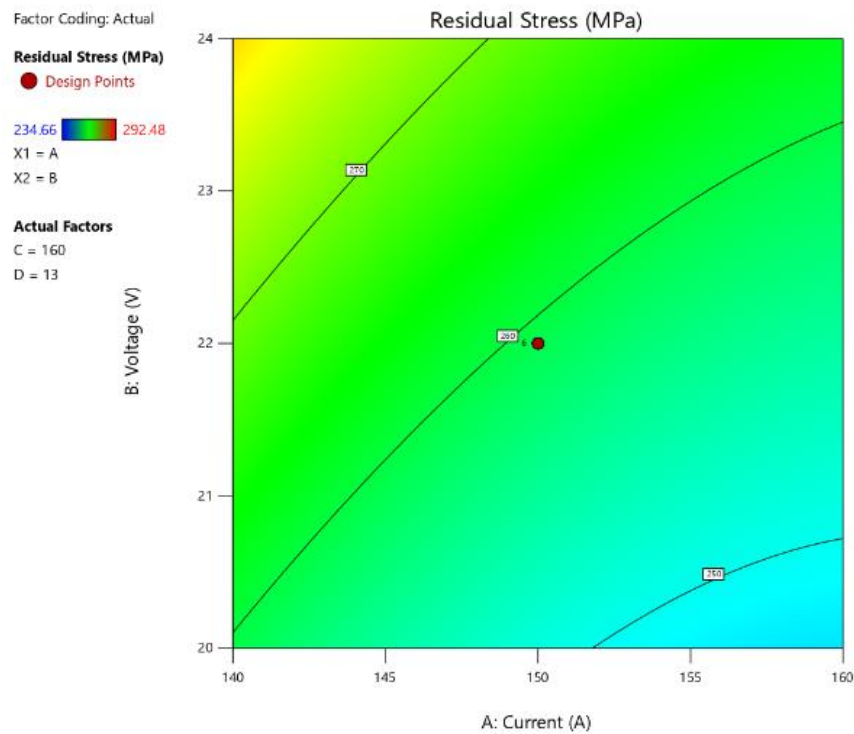


Figure 23. Contour plot for Residual Stress.

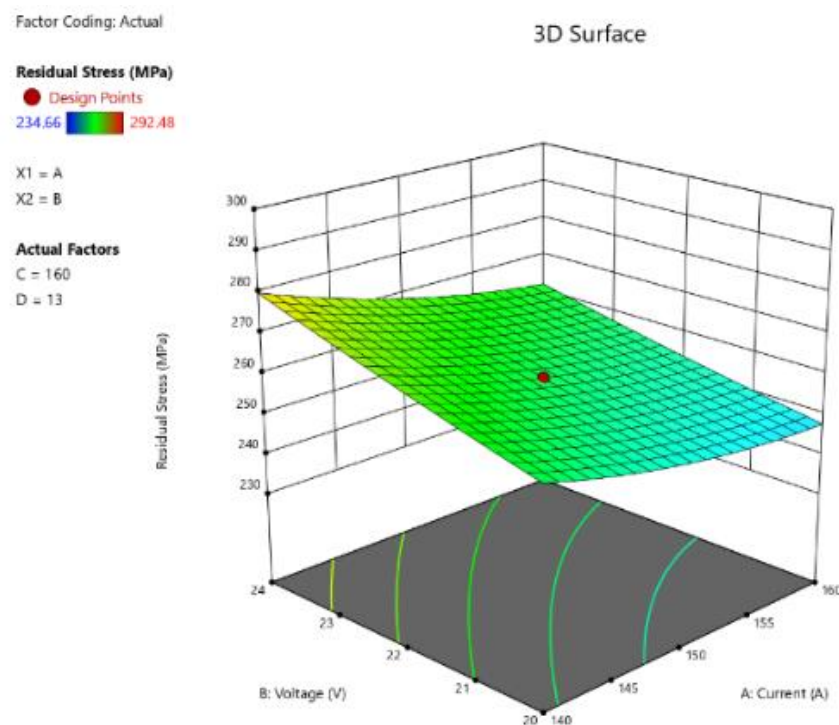


Figure 24. 3D surface plot for Residual Stress.

Figure 25 illustrates a contour plot revealing the distortion distribution in a weldment, offering insights into the spatial variation of distortion levels across the welded structure. Distortion, caused by thermal expansion and contraction during the welding process, can adversely affect the

dimensional accuracy and mechanical properties of welded components. The contour plot displays different distortion levels using varying colors or contour lines, with regions of higher distortion represented by warmer colors and regions of lower distortion by cooler colors. Understanding the

distortion pattern aids engineers in optimizing welding parameters and implementing corrective measures to mitigate distortion, ensuring the dimensional accuracy and structural integrity of welded assemblies. Figure 26 presents a 3D surface plot depicting the distortion in a welded structure. Welding induces thermal gradients and material shrinkage, resulting in deformation, which can compromise the structural integrity and dimensional accuracy of the welded components. This plot visualizes how distortion varies across the surface of

the welded structure, highlighting areas where significant deformation occurs. By analyzing this distribution, engineers can identify regions prone to distortion and develop strategies to minimize it during the welding process. Implementing corrective measures such as fixture design, welding sequence optimization, or pre-welding component manipulation can help mitigate distortion, ensuring that the final product meets dimensional specifications and performance requirements.

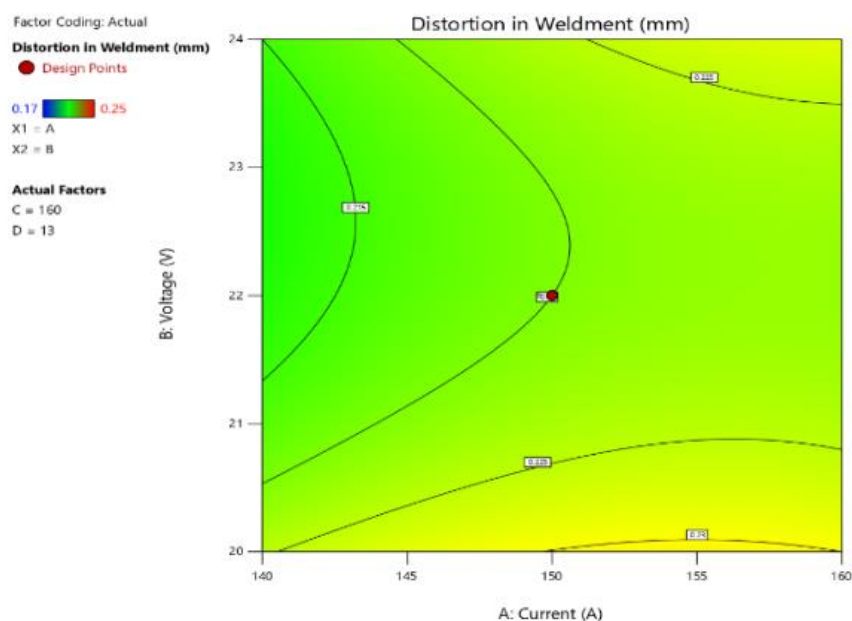


Figure 25. Contour plot for Distortion in Weldment.

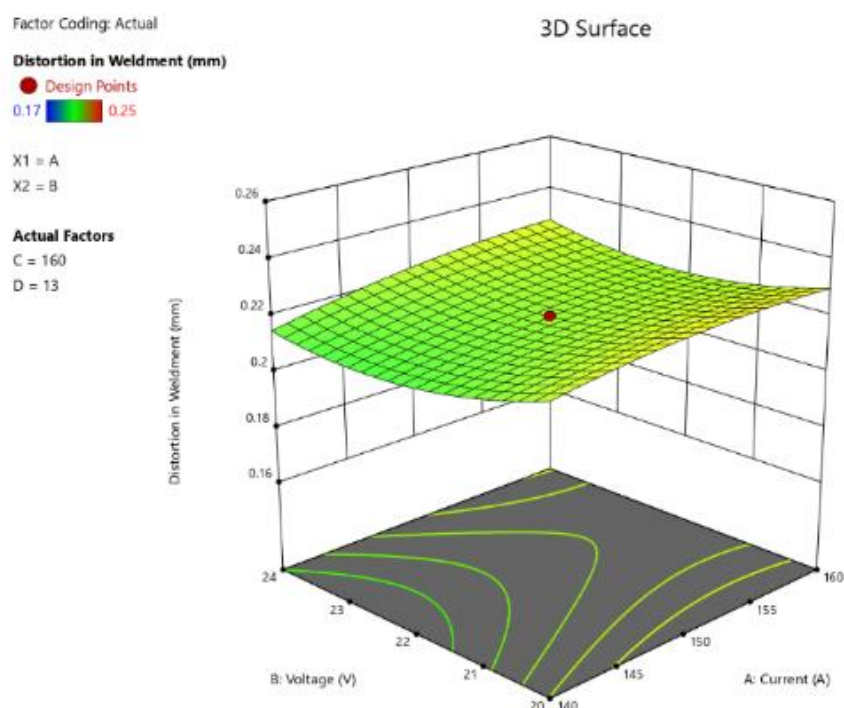


Figure 26. 3D plot for Distortion in Weldment.

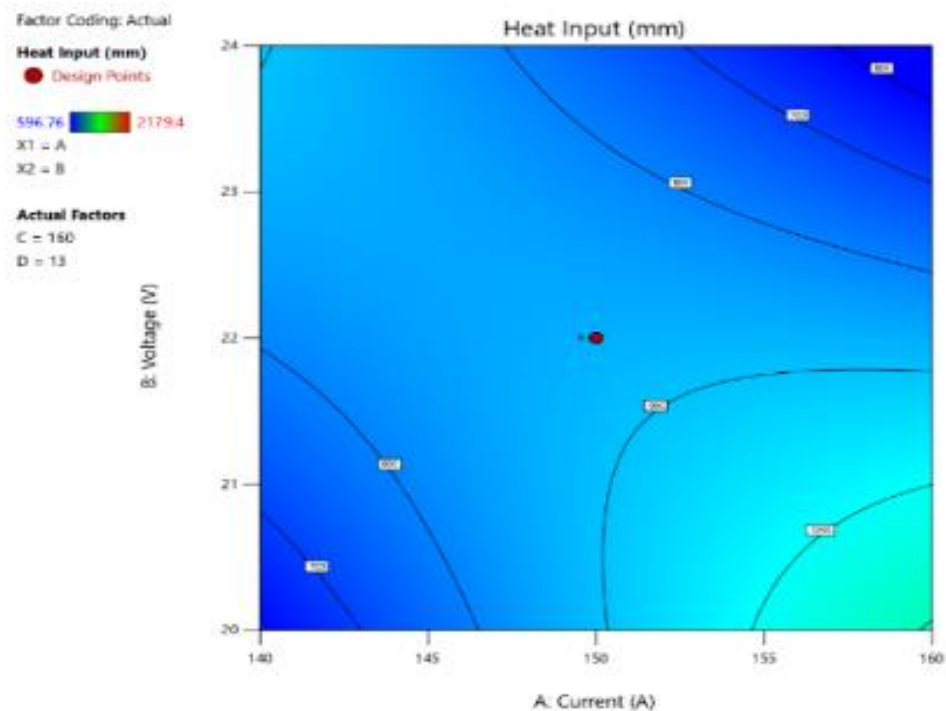


Figure 27. Contour plot for Heat Flux.

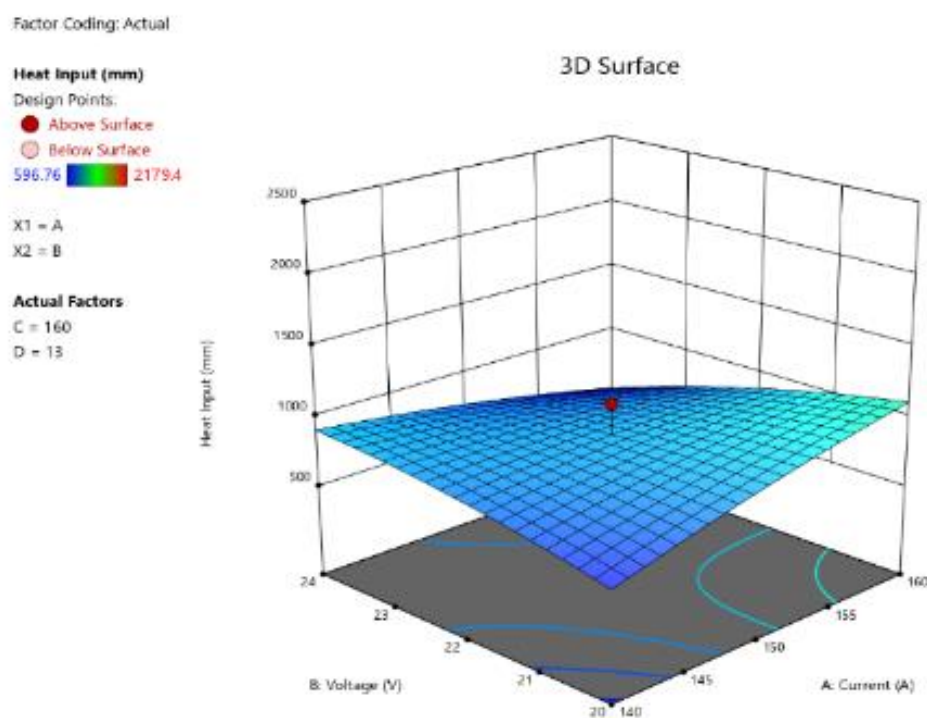


Figure 28. 3D surface plot for Heat Flux.

Figure 27 presents a contour plot illustrating the distribution of Heat Flux during welding processes. Heat Flux plays a critical role in determining the metallurgical characteristics and mechanical properties of welded joints. The contour plot visualizes the spatial variation of Heat Flux across the welded structure, with different regions

experiencing varying levels of Heat Flux represented by distinct colors or contour lines. Understanding the Heat Flux distribution enables engineers to optimize welding parameters, such as voltage, current, and travel speed, to achieve desired weld bead geometry, minimize distortion, and ensure adequate penetration and fusion between the base materials.

Additionally, controlling Heat Flux helps in managing microstructural changes, such as grain growth and phase transformations, which influence the mechanical performance and integrity of the welded components. Figure 28 illustrates a 3D surface plot representing Heat Flux distribution during a welding process. Heat Flux plays a crucial role in welding as it influences the material's microstructure, mechanical properties, and overall weld quality. This plot provides a visual representation of how heat is distributed across the welded joint, with different colors indicating varying levels of Heat Flux. Analyzing this distribution helps welders and engineers understand the thermal characteristics of the welding process and optimize parameters such as welding current, voltage, and travel speed to achieve desired weld properties.

By controlling Heat Flux, they can minimize issues like distortion, residual stresses, and metallurgical defects, ensuring high-quality welds and reliable performance of welded components.

Figure 29 depicts a contour plot showcasing the distribution of tensile strength across a welded structure. Tensile strength is a crucial mechanical property indicating the material's resistance to breaking under tension. This contour plot visualizes how tensile strength varies spatially within the weldment, providing insights into the effectiveness of the welding process and the quality of the resulting joints. Understanding the distribution of tensile strength helps engineers identify areas with potential weaknesses or defects, allowing for targeted improvements in welding parameters or post-weld heat treatments to enhance the overall mechanical integrity of the welded components. By optimizing tensile strength distribution, engineers can ensure that welded

structures meet performance requirements and exhibit reliable performance under applied loads. Figure 30 presents a 3D surface plot illustrating the distribution of tensile strength across a welded joint. Tensile strength is a critical mechanical property that indicates the material's ability to resist deformation or fracture under tension. This plot visually represents how tensile strength varies across the welded region, providing insights into the weld's structural integrity and load-bearing capacity. By examining this distribution, engineers can identify areas of potential weakness or variability in tensile strength, allowing them to optimize welding parameters and post-weld treatments to achieve uniform mechanical properties throughout the welded structure. This understanding is essential for ensuring the reliability and performance of welded components in real-world applications, particularly in industries where structural integrity is paramount, such as aerospace, automotive, and construction. Figure 31 illustrates the RSM (Response Surface Methodology) Ramps Optimization Diagram, which provides a visual representation of the optimal settings for various welding process parameters. The diagram shows how adjustments in parameters such as current, voltage, weld speed, and gas flow rate impact the response variables: Peak Temperature, residual stress, distortion in weldment, Heat Flux, and tensile strength. Each ramp on the diagram corresponds to a specific parameter and indicates the optimal levels that achieve the desired response. The intersection points on the ramps represent the exact values for each parameter to meet the optimization goals, allowing for a clear and comprehensive understanding of how each parameter influences the overall welding performance.

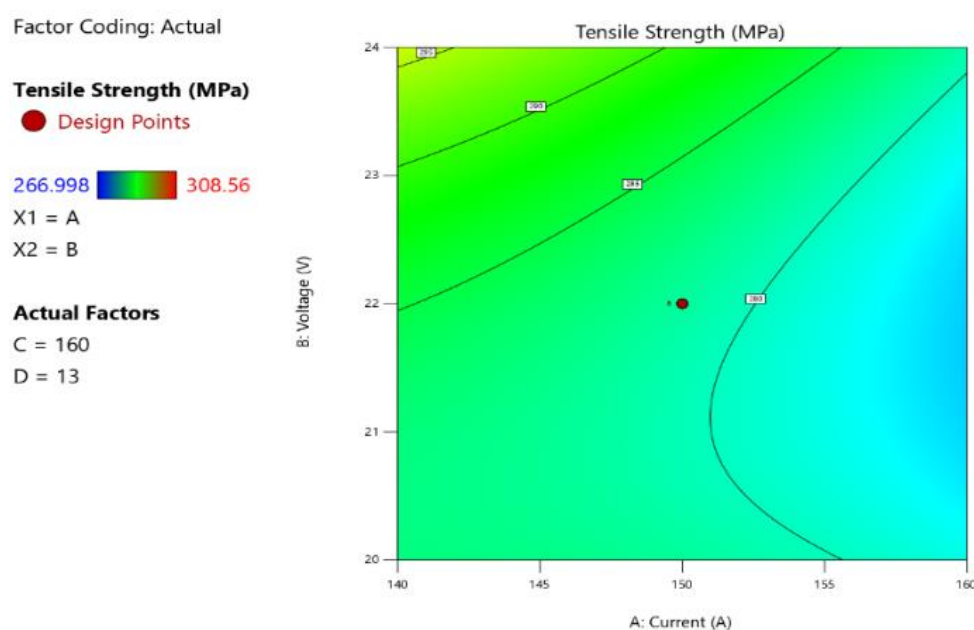


Figure 29. Contour plot for Tensile strength.

Factor Coding: Actual

Tensile Strength (MPa)

● Design Points

266.998 308.56

X1 = A

X2 = B

Actual Factors

C = 160

D = 13

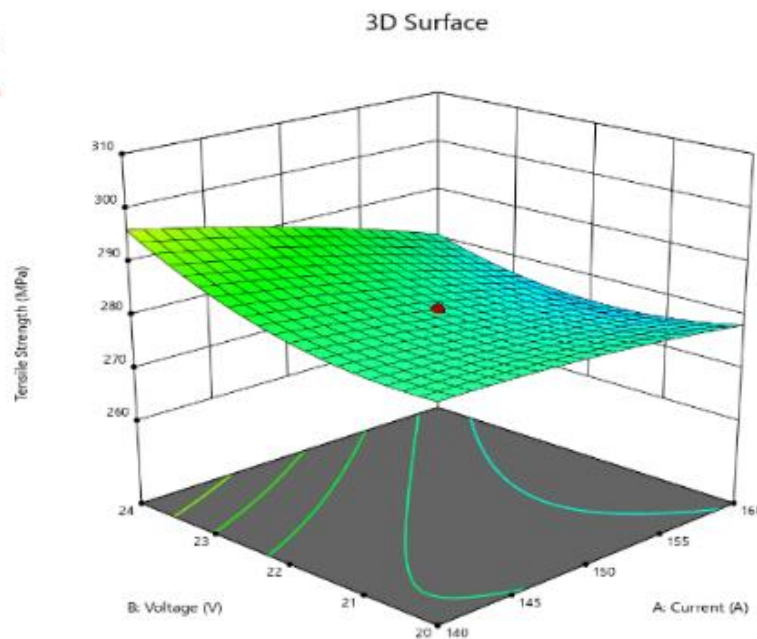
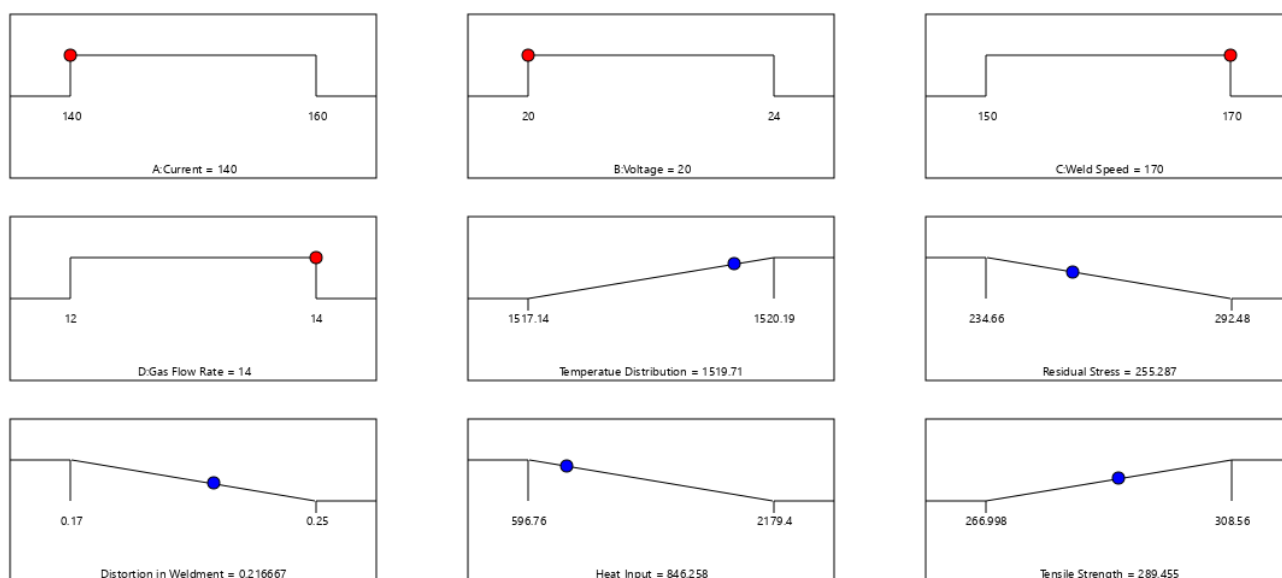


Figure 30. 3D surface plot for Tensile strength.



Desirability = 0.623
Solution 1 out of 100

Figure 31. RSM Ramps Optimization diagram.

Figure 32 presents a bar graph generated through Response Surface Methodology (RSM) for optimization purposes. This graph visually depicts the relationship between different optimization objectives and their corresponding desirability values. Each bar represents a specific optimization goal, such as maximizing tensile strength or minimizing residual stress, and the height of the

bar indicates the desirability score achieved for that particular objective. The graph provides a straightforward comparison of the desirability levels for each optimization goal, enabling a quick assessment of the overall effectiveness of the optimization process and helping identify which objectives have been successfully met or require further refinement.

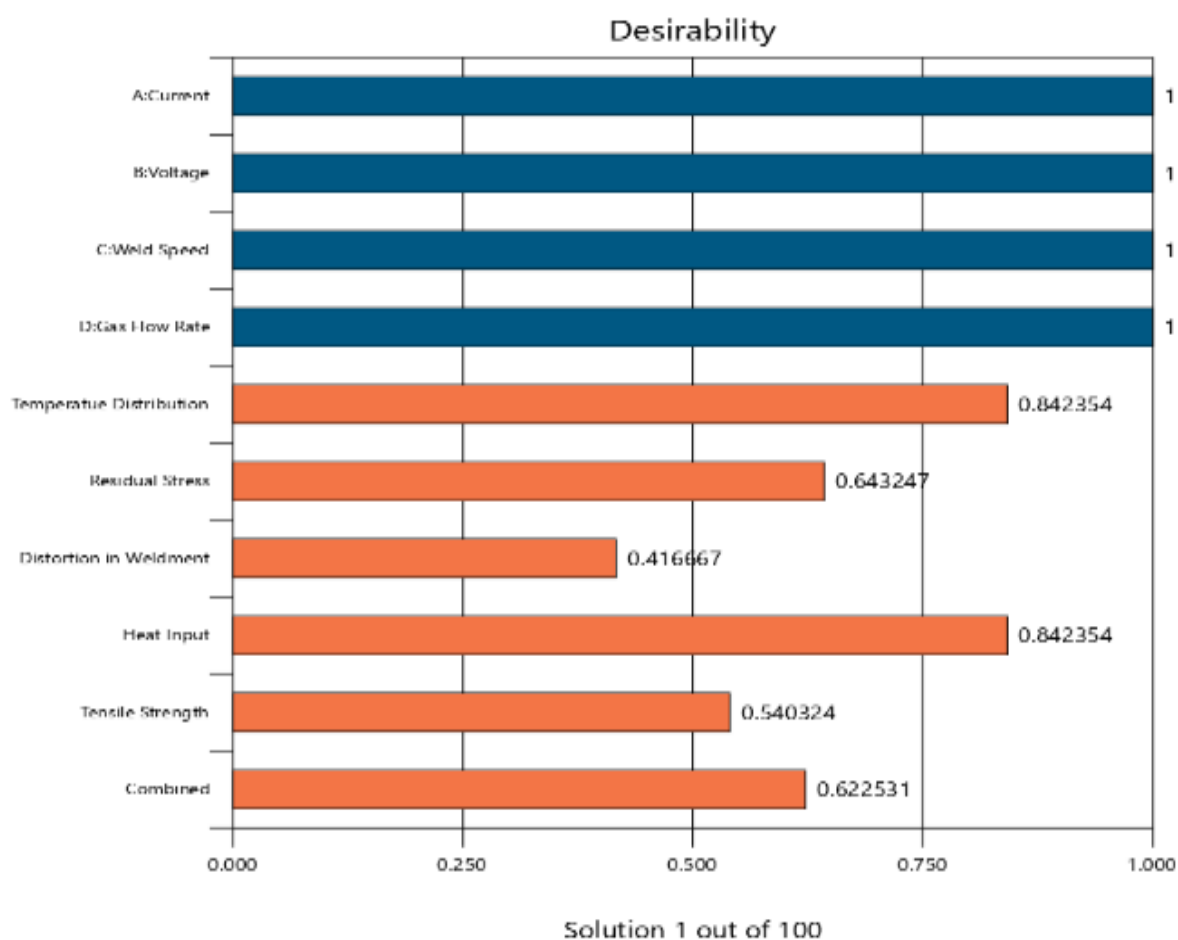


Figure 32. RSM Bar graph for Optimization.

5. Conclusion

RSM helps in understanding the effect of each parameter and their interactions on the responses. The fitted model was used to predict the optimal set of parameters that minimize or maximize the desired responses.

The results indicated model F-values of 29.81 at a P-value of <0.0001 for the tensile strength explained the significance of the employed model. Optimal tensile strength of 308.56Mpa, minimum distortion in weldment of 0.2, Peak Temperature of 1518.45oC, residual stress of 282.724Mpa and heat flux of 1500.26Kw/min were achieved with overall desirability Of 62.51% at a welding current of 140A, welding voltage 24V, gas flow rate 12lit/min and welding speed of 150 cm/min.

Overall, these statistics suggest that the regression model for the desired responses are robust and adequately captures the relationship with the predictor variables. In this case, the quadratic terms and the interactions which have significant p-values, suggest that they significantly contribute to the variability in the response variables.

In conclusion, this research has provided valuable insights into the optimization of welding parameters using Response

Surface Methodology (RSM) that can be effectively apply to drive innovation and competitiveness in the welding industry.

Acknowledgments

I sincerely wish to express my profound gratitude first of all to the Almighty GOD for the strength given me to carry out this researched work. Secondly my appreciation goes to my Supervisor Engr. Prof. Christopher Izelu for his distinguished supervision and review of my work, constantly inspiring and motivating me on this research. I also wish to thank my second supervisor and reviewer Dr. Benedict Omonigho Otanocha.

Author Contributions

Sunny Itaofu Iremia: Conceptualization, Formal Analysis, Investigation, Methodology, Project administration, Resources, Validation, Writing – original draft, Writing – review & editing

Izelu Christopher Okhechukwu: Supervision, Writing – review & editing

Omonigho Benedict Otanocha: Supervision

Conflicts of Interest

There is no conflict of interest. This is part of my researched thesis for my educational fulfilment.

References

- [1] Smith, J., et al. (2018). "Challenges in TIG Welding: An Overview." **Journal of Advanced Joining Processes**, 1, 100-110.
- [2] Johnson, M., & Lee, A. (2019). "Challenges and Solutions in TIG Welding of Mild Steel." **Welding International**, 33(5), 217-222.
- [3] Anderson, T., et al. (2020). "Assessing the Impact of Heat Flux on TIG Welded Mild Steel." **Journal of Material Science & Engineering**, 44(6), 755-764.
- [4] Singh, R., et al. (2021). "Effect of Welding Parameters on Mechanical Properties in TIG Welding of Mild Steel." **Materials Today: Proceedings**, 34(2), 517-524.
- [5] Harris, D., & White, P. (2022). "The Role of Computational Welding Mechanics in Modern Manufacturing." **International Journal of Advanced Manufacturing Technology**, 59(7-8), 1023-1039.
- [6] Kumar, R., & Patel, V. (2023). "Application of Optimization Algorithms in Welding: A Review." **Journal of Welding and Joining**, 41(1), 1-16.
- [7] H. K. Narang, U. P. Singh, M. M. Mahapatra and P. K. Jha. (2011). Prediction of the Weld Pool Geometry of TIG Arc Welding by Using Fuzzy Logic Controller. *International Journal of Engineering, Science and Technology*, 3(9), 77-85.
- [8] A L Dhobale and Prof H K Mishra (2015)" Review on Effect Of Heat Flux On Tensile Strength Of Butt Weld Joint Using Mig Welding "International Journal Of Innovations In Engineering Research And Technology [IJERT] ISSN: 2394-3696 volume 2, issue 9, sep.-2015.
- [9] Manabendra Saha, S. S. Dharmi. Effect of TIG Welding Parameter of Welded Joint of Stainless Steel SS304 by TIG Welding, *Trends in Mechanical Engineering & Technology* ISSN: 2231-1793 (Online), ISSN: 2347-9965 (Print) (2018) 18-27 Volume 8, Issue 3 www.stmjournals.com
- [10] Gurudatt Ghadi, Dr. Shivakumar S. Analysis of TIG Welding Process Parameters for Stainless Steel (SS202) *International Journal of Advanced Engineering Research and Science (IJAERS)* [Vol-3, Issue-10, Oct- 2016] <https://dx.doi.org/10.22161/ijaers/3.10.13> Page | 66.
- [11] G. Olabi, K. Y. Benyounis, M. S. J. Hashmi, Application of Rsm in Describing the Residual Stress Distribution in Co2 Laser Welding of Aisi304, *Strain Journal*, Vol. 43, No. 1, 2007, Pp. 37-46.
- [12] Paradowska, T. R. Finlayson, J. W. H. Price, R. Ibrahim, A. Steuwer, and M. Ripley, "Investigation of reference samples for residual strain measurements in a welded specimen by neutron and synchrotron X-ray diffraction," *Physica B*, vols. 385-386, 2006, pp. 904-907.
- [13] Raveendra, Dr. B. V. R. Ravi Kumar, Dr. A. Sivakumar, N. santhosh "Effect of welding parameters on 5052 aluminium alloy weldments Using TIG welding" *International Journal of Innovative Research in Science, Engineering and Technology (An ISO 3297: 2007 Certified Organization)* Vol. 3, Issue 3, March 2014.
- [14] Achebo Joseph & Omoregie Monday (2015). Application of Multi-Criteria Decision Making Optimization Tool for Determining Mild Steel Weld Properties and Process Parameters Using the TOPSIS. *International Journal of Materials Science and Applications*. Vol. 4, No. 3, 2015, pp. 149-158. <https://doi.org/10.11648/j.ijmsa.20150403.12>
- [15] Ambroziak, M. Korzeniowski, P. Kustroń, "Friction welding of dissimilar metal joints with intermediate layers", *Journal of Achievements in Material and Manufacturing Engineering (AMME)*, Volume 21, Issue 2, April 2007.
- [16] Amit Kumar, M. K. Khurana And Pradeep K. Yadav (2016)"Optimization Of Gas Metal Arc Welding Process Parameters "Materials Science And Engineering 149 (2016) 012002.
- [17] Anawa EM, Olabi AG, Hashmi MSJ. Optimization of ferritic/austenitic laser welded components. In: Presented at AMPT2006 international conference July 30–August 3, 2006, Las Vegas [NV], USA, 2006.
- [18] Owunna Ikechukwu Bismarck, Ikpe Aniekan Essienubong, Experimental and Numerical Optimization of Tungsten Inert Gas (TIG) Welding Process Parameters Relative to Mechanical Properties of AISI 1018 Mild Steel Plate. *Advances in Engineering Design Technology* Vol. 3, 2021 pp. 132-145.
- [19] AMADHE, F. O. 1,*, ACHEBO, J. I., OBAHIAGBON, K., OZIGAGUN, A. Application of Numerical and Computational Based Models for Modelling the Effects of the Electrode Density in Mild Steel TIG Welding Process, *FUPRE Journal of Scientific and Industrial Research* 7(3): 108-121 (2023).
- [20] Kora T Sunny, Nanda Naik Korra, M Vasudevan and B Arivazhagan Parameter optimization and experimental validation of A-TIG welding of super austenitic stainless steel AISI 904L using response surface methodology, *Proceedings of the Institution of Mechanical Engineers, Part E: Journal of Process Mechanical Engineering*, Restricted access Research article First published online May 9, 2022. <https://doi.org/10.1177/0954408922109567>
- [21] Anne Auger and Olivier Teytaud (2008). Continuous Lunches Are Free Plus the Design of Optimal Optimization Algorithms. *Algorithmica*, May 2010, Volume 57, Issue 1, Pp 121–146, 25 October 2008.
- [22] ANSI/AWS Z49.1: "Safety in Welding, Cutting, and Allied Processes" (2005).
- [23] ApurvChoubey, Vijayku mars. Jatti (2014), Influence of Heat Flux on mechanical properties and microstructure of Austeritic 202 grade stainless steel weldment; *WSEAS TRANSACTION on Applied and Theoretical Mechanics*. 9: 2224 – 3429.

- [24] Armstrong, Jon Scott (2001). "Role playing: a method to forecast decisions". In Armstrong, Jon Scott. Principles of forecasting: a handbook for researchers and practitioners. International series in operations research & management science. Boston, MA: Kluwer Academic Publishers. pp. 15–30. https://doi.org/10.1007/978-0-306-47630-3_2
- [25] Arpita N. Bhavsar, Vikram A. Patel (2016) "Influence of process parameters of TIG welding process on mechanical properties of SS304L welded joint" International Research Journal of Engineering and Technology (IRJET) Volume: 03 Issue: 05 May-2016.
- [26] Sindiri Mahesh and Velamala. Appalaraju "Optimization of MIG Welding Parameters for Improving Strength of Welded Joints" (IJITR) International Journal of Innovative Technology and Research Volume No. 5, Issue No. 3, April – May 2017, 6453–6458. 2320–5547@ 2013-2017 <http://www.ijitr.com> All rights Reserved Page | 6453.
- [27] Capello E., Colombod. And Previtali B. (2005). "Repairing of Sintered Tools Using Laser Cladding By Wire", Journal Of Materials Processing Technology, Volumes 164–165, 15 May 2005, Pages 990-1000, <https://doi.org/10.1016/J.Jmatprotec.2005.02.075> get Rights And Content.
- [28] Cary & Helzer (2005), Electric Arc, pp. 4, 20, 24 and 94. D. Van Nostrand Co., New York, 1902.
- [29] Casalino G, Hu Sj, Hou W. Deformation Prediction and Quality Evaluation of the Gas Metal Arc Welding Butt Weld. J Eng Manuf 2003; 217(Part B): 1615–22.
- [30] Cengiz S, Azakli Y, Tarakci M, Stanciu L, Gencer Y (2017). Microarc Oxidation Discharge Types and Bio Properties of the Coating Synthesized On Zirconium. Mater Sci Eng C Mater Biol Appl. 77: 374-383. <https://doi.org/10.1016/J.Msec.2017.03.230>
- [31] V. M. Joy Varghese, M. R. Suresh, D. Siva Kumar, Recent developments in modeling of heat transfer during TIG welding - A review. February 2012. The International Journal of Advanced Manufacturing Technology 64(5-8). <https://doi.org/10.1007/s00170-012-4048-9>
- [32] Chance, Beth L.; Rossman, Allan J. (2005). "Preface". Investigating Statistical Concepts, Applications, and Methods. Duxbury Press.
- [33] Chang, W. S. and Na, S. J., (2002), A study on the prediction of the laser weld shape with varying heat source equations and the thermal distortion of a small structure in micro-joining, Journal of Material Processing Technology, Vol. 120 (1–3), pp 208–214.
- [34] Chantrelle Fp, Lahmidi H, Keilholz W, El Mankibi M, Michel P. Development of A Multicriteria Tool for Optimizing the Renovation Of Buildings. Appl Energy 2011; 88(4): 1386e94.
- [35] Chatzinikolaidou M., Laub M., Rumpf H., Jennissen H. P., (2002). Biocoating of Electropolished and Ultra-Hydrophilic Titanium and Cobalt Chromium.
- [36] Chatzinikolaidou M., Zumbrink T., And Jennissen H. P., (2003). Stability of Surface-Enhanced Ultrahydrophilic Metals as A Basis for Bioactive Rhbmp-2 Surfaces. First Published: December 2003; <https://doi.org/10.1002/Mawe.200300714> Volume 34, Issue 12; December 2003, Pages 1106–1112.
- [37] Palani, P. & Saju, Manirul. (2013). Modelling And Optimization Of Process Parameters For Tig Welding Of Aluminium-65032 Using Response Surface Methodology. International Journal of Engineering Research and Applications. 3. 230-236.